Biomaterials 281 (2022) 121352

Contents lists available at ScienceDirect

Biomaterials

journal homepage: www.elsevier.com/locate/biomaterials

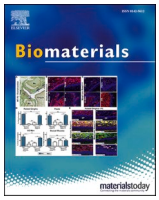

Subdural neural interfaces for long-term electrical recording, optical microscopy and magnetic resonance imaging

Xiaomeng Wang [a,b,1], Mengqi Wang [c,1], Hao Sheng [e,1], Liang Zhu [c,d], Junming Zhu [a], Hequn Zhang [c], Yin Liu [c], Li Zhan [a,b], Xi Wang [a,b], Jiaozhen Zhang [a,b], Xiaotong Wu [a,b], Zhigang Suo [e,***], Wang Xi [c,d,**], Hao Wang [a,b,*]

[a] Department of Neurobiology and Department of Neurosurgery of Second Affiliated Hospital, Key Laboratory for Biomedical Engineering of Education Ministry, Zhejiang University School of Medicine, Hangzhou, Zhejiang, 310058, China
[b] NHC and CAMS Key Laboratory of Medical Neurobiology, MOE Frontier Science Center for Brain Research and Brain Machine Integration, School of Brain Science and Brain Medicine, Zhejiang University, Hangzhou, Zhejiang, 310058, China
[c] Interdisciplinary Institute of Neuroscience and Technology, Department of Anesthesiology, The Second Affiliated Hospital, School of Medicine, Zhejiang University, Kaixuan Road 258th, Hangzhou, Zhejiang, 310020, China
[d] Key Laboratory of Biomedical Engineering of Ministry of Education, College of Biomedical Engineering and Instrument Science, Zhejiang University, Hangzhou, Zhejiang, 310027, China
[e] School of Engineering and Applied Sciences, Kavli Institute of Bionano Science and Technology, Harvard University, Cambridge, MA, 02138, United States

ARTICLE INFO

Keywords:
Electrocorticogram
Hydrogel-elastomer neural interface
Multi-model
Biocompatibility
Two-photon imaging
Magnetic resonance imaging

ABSTRACT

Though commonly used, metal electrodes are incompatible with brain tissues, often leading to injury and failure to achieve long-term implantation. Here we report a subdural neural interface of hydrogel functioning as an ionic conductor, and elastomer as a dielectric. We demonstrate that it incurs a far less glial reaction and less cerebrovascular destruction than a metal electrode. Using a cat model, the hydrogel electrode was able to record electrical signals comparably in quality to a metal electrode. The hydrogel-elastomer neural interface also readily facilitated multimodal functions. Both the hydrogel and elastomer are transparent, enabling *in vivo* optical microscopy. For imaging, cerebral vessels and calcium signals were imaged using two-photon microscopy. The new electrode is compatible with magnetic resonance imaging and does not cause artifact images. Such a new multimodal neural interface could represent immediate opportunity for use in broad areas of application in neuroscience research and clinical neurology.

1. Introduction

In subdural electrophysiology, electrodes are inserted between the dura mater and cortical surface ([1,2]). These subdual electrodes are used as diagnostic tools for diseases such as epilepsy and brain tumors ([3,4]), or can be used as brain-machine interfaces for artificial limbs ([5–8]) ([9]). Subdural electrodes in clinical practice are usually made of metals ([10]). These do not often conform well to the curved surface of the brain, and may shift and injure the brain as the brain pulsates or when the patient moves ([11–13]). Subdural electrodes have also been developed using micro-fabricated materials ([14–18]). However, these electrodes are still far stiffer than brain tissue and are similarly unsuitable for long-term implantation ([19–21]).

Recently, we and others have explored hydrogels as electrodes ([22–25]). A hydrogel can be fabricated with a polymer network and artificial cerebrospinal fluid (ACSF). The ACSF mimics the liquid around brain tissues and conducts electricity using ions. The hydrogel electrode can be made compatible with brain tissues mechanically, electrically,

* Corresponding author. Department of Neurobiology and Department of Neurosurgery of Second Affiliated Hospital, Key Laboratory for Biomedical Engineering of Education Ministry, Zhejiang University School of Medicine, Hangzhou, Zhejiang, 310058, China.
** Corresponding author. Interdisciplinary Institute of Neuroscience and Technology, Department of Anesthesiology, The Second Affiliated Hospital, School of Medicine, Zhejiang University, Kaixuan Road 258th, Hangzhou, Zhejiang, 310020, China.
*** Corresponding author.
E-mail addresses: suo@seas.harvard.edu (Z. Suo), xw333@zju.edu.cn (W. Xi), haowang@zju.edu.cn (H. Wang).
[1] These authors contributed equally to this work.

https://doi.org/10.1016/j.biomaterials.2021.121352
Received 26 August 2021; Received in revised form 23 December 2021; Accepted 27 December 2021
Available online 30 December 2021

and chemically ([26–29]).

Multimodal neural interfaces are under intense development ([16,30–35]). However, since the metal blocks light and is prone to photoelectric artifacts that can interfere with physiological signals, metal electrodes have limited applicability for simultaneous electrical recording with optical microscopy or optogenetic stimulation ([36,37]). Some improvements were facilitated using graphene microelectrodes which are transparent, and enabled simultaneous electrical recording and optical microscopy ([38,39]). However, these electrodes remain the problem of stiffer than brain tissue. In addition, it is highly desirable to make subdural electrodes compatible with magnetic resonance imagining (MRI), but few examples such as graphene-based interfaces have yet materialized ([40]).

Here we develop a hydrogel-elastomer neural interface (HENI) to enable electrophysiology, optical microscopy, and magnetic resonance imagining (Fig. 1A). The neural interface consists of hydrogel electrodes and interconnections, together with elastomer dielectrics (Fig. 1B). The PVA-ACSF hydrogel and neural tissues have comparable elastic moduli (PVA-ACSF: 1.3 KPa; white mater and grey matter: 300 Pa and 450Pa, respectively ([41])) and water content (PVA-ACSF: 90% (wt%); white mater and grey matter: 71% and 83%, respectively ([26,27])), while the elastomer (1 MPa) and dura mater (~1 MPa) have comparable elastic moduli (Fig. 1C) [24,29,42]. The softness of the hydrogel and elastomer enables the interface to conform to the curved surface of the brain. The neural interface can collect electrophysiological signals over a long period (28 days) with low immune responses and only minor cerebrovascular destruction. We demonstrate that a hydrogel electrode and a metal electrode record electrophysiological signals of comparable quality. Both the hydrogel and elastomer are transparent, enabling simultaneous electrical recording and optical microscopy. Over the wavelength range from 350 nm to 1350 nm, the optical transmittance of a 400 μm-thick hydrogel is similar to that of ACSF solution (Fig. 1D). The average transmittance of the hydrogel is 86.22% over the visible wavelength range (390–750 nm). The hydrogel-elastomer neural interface is compatible to MRI and does not cause artifact images. The multimodal neural interface opens opportunities for advancing the tools of neuroscience research and clinical neurology.

2. Materials and Methods

2.1. Animals

For cats, adult healthy male cats (n = 5, 4–5 years old and weighing 3–4 kg) were used. Three cats were used for electrophysiological recording (among them, two cats were used for ECoG (Electrocorticography) recording, and one cat was used for electro-stimulation experiment), one cat for MRI imaging and one cat for NIR-II microscopy imaging. For mice, male C57BL/6J mice (n = 6) at the age of 2–6 months were obtained from the Shanghai Laboratory Animal Center and used for electrophysiological recording and optical imaging experiments. All experimental procedures conducted in cats and mice were approved by the Institutional Animal Care and Use Committee of Zhejiang University and in accordance according to the guidelines of the International Council for Animal Care. During experiments, all animals were housed at the Cat Room or Mouse Room at Zhejiang University animal center and fed with food and water ad libitum, under 22 ± 1 °C and 55 ± 5% humidity and 12-h light/dark cycle.

2.2. Hydrogel-elastomer neural interface materials and fabrication

The hydrogel-elastomer neural interface was designed and fabricated with the PVA-ACSF hydrogel as a conductive material and PDMS as a dielectric shell. The generic fabrication process was mainly divided into three components and detailed below:

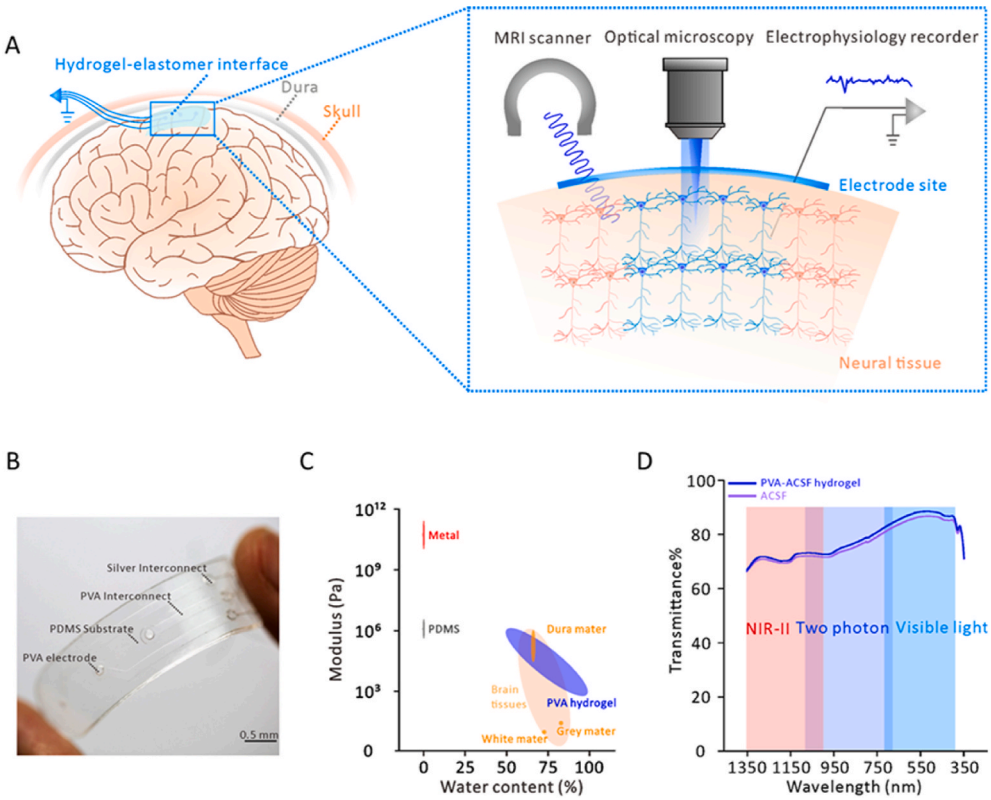

Fig. 1. A subdural hydrogel-elastomer neural interface enables multimodal functions. (A) The interface implanted between the cortical surface and the dura mater enables electrical recording, optical microscopy, and magnetic resonance imaging. (B) A photo of the hydrogel-elastomer neural interface. (C) Elastic moduli and water content of various materials. (D) Transmittance of a 400 μm-thick hydrogel at various wavelengths.

2.2.1. Fabrication of PDMS dielectric shell

The PDMS precursor was a mixture of pre-polymer and cross-linker at 10:1 (w:w, Sylgard 184, Dow Corning). We customized two kinds of metal model. The metal model for casting PDMS substrate was curved into specific patterns with electrodes holes, grooves for hydrogel interconnects and pillars for silver interconnects. The other metal model was prepared for casting PDMS cover. Both metal models were made of aluminum alloy. With the help of specific-sized acrylic cover, the PDMS substrate was at 300 μm thick and the PDMS cover was at 150 μm thick. The PDMS substrate and cover were then cured for 4–5 h at 80 °C to crosslink the PDMS precursor. After crosslink completion, the PDMS substrate and cover were removed from the metal models and silver rings were manually embedded into the pillars at the end of each channel (see Fig. 2A and B). Next, a thin layer of PDMS precursor was spin-coated on the PDMS cover to adhere to the PDMS substrate (Spin Processor: Yingjia electron). Finally, the pre-PDMS dielectric shell was cured for 4–5 h at 80 °C again to crosslink the PDMS precursor for adhering the cover to the substrate. The whole PDMS dielectric shell was at 500 μm thickness.

2.2.2. The fabrication of PVA-ACSF hydrogel

We used the artificial cerebrospinal fluid (ACSF) as the solvent of the hydrogels and polyvinyl alcohol (PVA) as the polymer. ACSF used in our experiments contained (in mM): 125 NaCl (Sigma, S5886), 2.5 KCl (Sigma, P5405), 2 $CaCl_2{\cdot}H_2O$ (Sigma, C3881), 1.3 $MgCl_2{\cdot}6H2O$ (Sigma, M0250), 1.3 NaH_2PO_4 (Sigma, 71,505), 25 $NaHCO_3$ (Sigma, 792,519), 10 glucose (Sigma, G6152). All solutes were fully dissolved in deionized water.

To synthesize the PVA-ACSF hydrogel, we first dissolved 10g PVA pre-polymer (ALDRICH, BCBT7691) in 90 mL ACSF and stirred the solution for 30 min. For complete dissolution we cured the mixture overnight in a convection oven (80 °C). The transparent solution of PVA pre-polymer and ACSF was used as the precursor of PVA-ACSF hydrogel. Finally, we frozen and thawed the solution to crosslink the PVA precursor as hydrogel.

2.2.3. The fabrication of hydrogel-elastomer neural interface

We submerged the whole PDMS dielectric shell into the precursor of PVA-ACSF hydrogel, drew the precursor into the precursor using a vacuum pump, and gelled the precursor of PVA-ACSF hydrogel by freezing (−20 °C for 30mins) and thawing.

2.3. The transmittance of the PVA-ACSF hydrogel

The transmittance of the PVA-ACSF hydrogels was measured by a spectrophotometer (Agilent technologies). A 500 μm thick section of PVA-ACSF hydrogel was tested with the transmittance at a 350–1350 nm wavelength, and with a control of a 500 μm thick section of ACSF.

2.4. The conductivity of the hydrogel-elastomer neural interface

We first prepared the hydrogel-elastomer neural interface in saline (0.9% (wt%) NaCl in water). Under saline, we then connected the input of an oscilloscope (Blackrock, US) through the hydrogel electrode to the output of a signal stimulator (AM-system, Model 2100) and connected their grounds. After that, we used the stimulator to output sinusoidal waves of ±100 mV (scale of the polarization voltage of neurons) of different frequencies and checked detective waves on the oscilloscope.

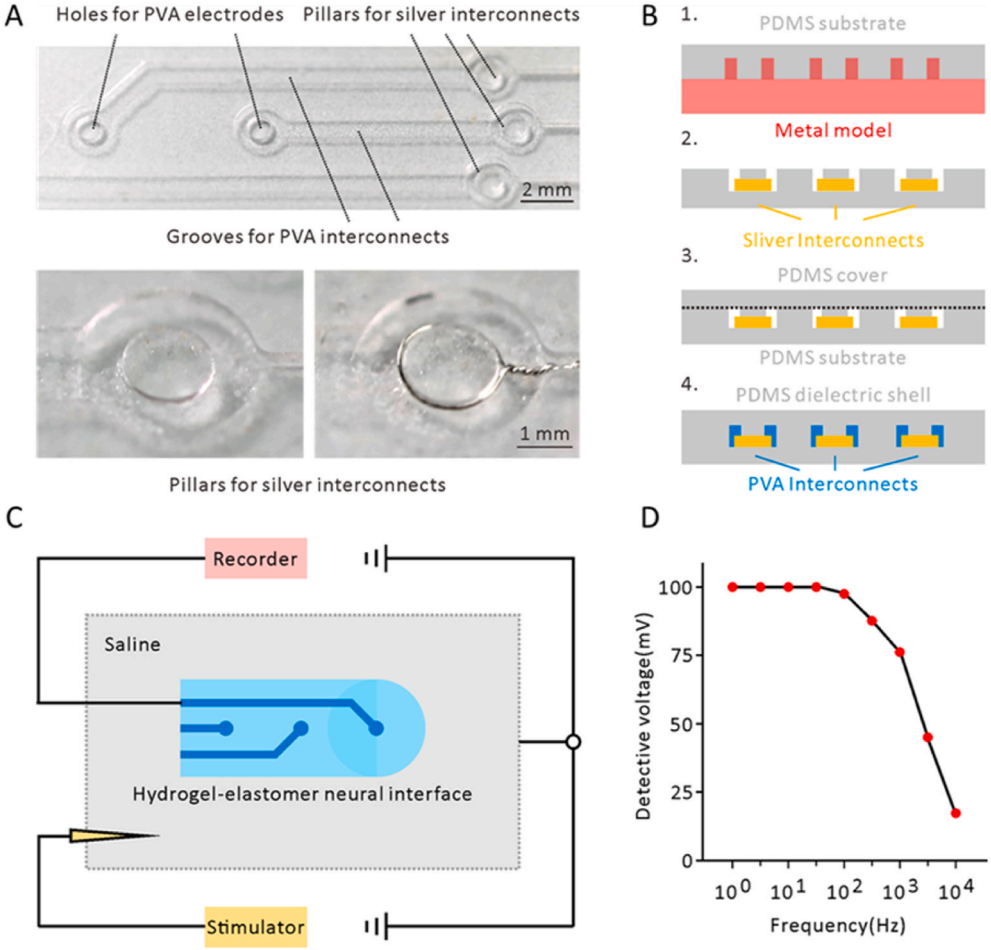

Fig. 2. The fabrication and electrical characterization of hydrogel-elastomer neural interface.

2.5. Animal surgical procedure

Cats were anesthetized with ketamine hydrochloride (10 mg/kg)/ atropine (0.03 mg/kg) and maintained with propofol (3–10 mg/kg per hour i. v.) or sufentanil (2–4 μg/kg per hour i. v.) supplemented with isoflurane (0.5–2%). Animals were intubated and artificially ventilated. End-tidal CO_2, respiration rate, SpO_2, heart rate, electrocardiogram and rectal temperature were continuously monitored and maintained. The end-tidal CO_2 was kept around 4% by adjusting the rate and volume of the ventilator, and the rectal temperature of 37.5 °C–38.5 °C was maintained via an animal warming system.

2.6. Electrophysiology recording

In the electrophysiological recording experiment, three cats were implanted with hydrogel-elastomer neural interface and metal electrodes. After removing the skull, the dura mater was picked up under a microscope and cut in a vertical direction. The hydrogel-elastomer neural interface was placed on the cortex surface and the silver wire at the tail end for external connection. Then the skull was covered back to its original position and sealed with sterilized dental cement to fix the electrode. The commercial metal electrode was fixed on the contralateral cortical surface using the same procedure. A small hole was made in the front of the skull and a screw fixed into the skull slowly. Then a copper wire was wrapped around the exposed screw as a reference line for electrophysiological recording. Finally, the wound was sutured, and lidocaine ointment applied for pain relief.

For the ECoG recording experiments, isoflurane (ISO) (0.5–0.8% and 2%) and propofol (3–5 mg/kg/h and 10 mg/kg/h) were used to maintain the different anesthesia states of animal. The ECoG signals were recording by the Cerebus neurophysiological signal acquisition system (Blackrock, US). The silver wires exposed on the cat's head were connected to a 32-channel headstage connected to the pre-signal amplifier. Electrophysiological signals were recorded simultaneously by hydrogel and metal electrodes. After being amplified, the signals were recorded to the Cerebus system. All recorded electrical signals were amplified 1000X and then filtered at 0.1–10 kHz. For ECoG data analysis, the signals were filtered with low-pass filtering (1–500hz), and with sampling frequency at 1 kHz.

For the cat electro-stimulation experiment, we placed the stimuli tungsten electrode which links to an isolated pulse stimulator (AM-system, Model 2100) into the cortex surface fixed with dental cement, and placed it around 1 cm from the front side of metal electrodes. The stimulation duration was 150 ms and consisted of a train of 30 electrical pulses (200 Hz, 300 μs, 100 μA, biphasic +/−), the stimulus trial consisting of a 5s baseline period, 150 ms stimulation events, and 25s convalescence time for each trial of 30s. The cat received 20 electro-stimulation trails. At the same time, the ECoG signals were recorded to Cerebus system.

The mice front-paw electro-stimulation was performed as previously described on the ipsilateral side of the recorded sensorimotor cortex ([43]). The multi-pulse stimulation duration was 3s and consisted of a train of 9 electrical pulses (3 Hz, 100 μs, 0.3 mA, biphasic +/−) and a single-pulse stimulation (1s with 1Hz, 100 μs, 0.3 mA, biphasic +/−) delivered to a forepaw in anesthetized mice through a pair of thin needles implanted under the skin via an isolated pulse stimulator (AM-system, Model 2100). The intensity was adjusted to provide stimulation below the movement threshold. The stimulus trial consists of a 3s baseline period, 3s stimulation events, and 24s convalescence periods for each trial of 30s. Each mouse received 8 electro-stimulation trails. The two-photon microscope was responsible for sending a signal to the isolated pulse stimulator to synchronize electro-stimulation with imaging.

2.7. NIR-II fluorescence wide-field microscopic imaging

In the NIR-II fluorescence imaging experiment, a quartz glass window was made according to a previous procedure ([44]). A quartz glass coverslip (diameter = 12 mm, thickness = 0.17 mm) was glued into a metal ring (diameter = 8 mm, thickness = 2 mm) using silicone adhesive. The skull and dura were opened to expose the cortex. The edge of the glass was inserted under the dura and the metal ring was glued to the skull with dental cement to form an imaging chamber. Before NIR-II fluorescence imaging, Indocyanine green (ICG) was injected intravenously through the saphenous vein (~2 mg/kg) to label cerebral vessels. After completion of surgical and experimental procedures, analgesics were given to the animals and time given for recovery.

A previously lab-built optical system was established to conduct NIR-II fluorescence wide-field microscopic brain imaging on the cats. A 780 nm LED (M780L3-C1, Thorlabs, USA) was used as the excitation source. Reflected by a 900 nm long-pass (LP) dichroic mirror (DMLP900R, Thorlabs) and passing through an air objective lens (LSM03, with a working distance (WD) of 25.1 mm, Thorlabs) or an infrared anti-reflection water-immersed objective lens (XLPLN25XWMP2, 25 ×, numerical aperture (NA) = 1.05, Olympus, Japan), a 780 nm beam was illuminated onto the brain of the cat. The excited NIR-II fluorescence was collected using the same objective lens, passing through the same 900 nm LP dichroic mirror and a 900 nm LP filter (FELH0900, Thorlabs), and finally recorded using an InGaAs camera (SW640, Tekwin, China) via a built-in tube lens in a triocular (BX51, Olympus). The objective was fixed on a motor-driven electric module (ZFM2020, Thorlabs) and could be moved in the Z axis to focus at different depths of the brain. The whole microscope was fixed on a multi-directional adjustable shelf, which permitted careful positioning of the objective right above the window. A flexible translation and rotation system permitted precise positioning of the microscope perpendicular to the cranial window. In addition, placement of the cat on an independently controlled stage provided precise x-y movement when conducting imaging.

2.8. Immunohistochemistry

After implantation of two types of electrodes for 2 weeks, 3 weeks, 4 weeks and 14 weeks the cats were deeply anesthetized with sodium pentobarbital (1% wt/vol) and transcranial perfused with saline buffer followed by paraformaldehyde (4% wt/vol) in 0.1 M phosphate buffer. Then the brain was removed into 4% paraformaldehyde buffer for 6–8 h fixation at 4 centigrade. Next, the brain was dehydrated with 25% sucrose (wt/vol) overnight. Finally, coronal cryo-sections were cut at 40 μm on a freezing microtome (Thromo NX50) for confocal imaging and immunostaining. After being gently rinsed within 0.1 M phosphate buffer (3 × 10min) and ice-cold methanol (1 × 10min) and blocked with 5% (wt/vol) normal bovine serum (BSA) for 1 h at room temperature (RT), the brain slices were incubated with one of the following primary antibodies: anti-GFAP (mouse 1:200, Jackson lab) and anti-Iba1 (rabbit, 1:400, Wako) at 4 °C overnight. Next day, the sections were rocked and washed 3 × 10min in 0.1 M phosphate buffer and then incubated with fluorophore-conjugated secondary antibody for 2 h at RT (1:800: Millipore). Antibodies were diluted in phosphate-buffered saline containing 5% BSA. Finally, all images were acquired with 20 × or 40 × objectives using an Olympus FV3000 confocal microscope. For counting the number of glia cells, we applied double-blind trials and counted 12–14 brain slices for each cat.

2.9. Two-photon imaging

For the Mice Calcium Imaging, before electrode implantation, the mice received an intra-cortical injection of the genetically encoded calcium indicator GCaMP6s, targeted to neurons (rAVV2/9-hSyn-GCaMP6s-WPRE, 1.2×10^{13}) after craniotomy. A total volume of 1 μL of viral vector was manually injected through a patch pipette (tip diameter

of approximately 5–10 μm) at 0.3 mm and 0.6 mm depth below the pial surface.

Mice with a craniotomy window were mounted and immobilized to a stationary apparatus and were imaged using TPM in an anesthetized state (1–3% isoflurane). Just before imaging, the mice were anesthetized with isoflurane and retro-orbitally injected with 0.2 mL 70 kDa Texas Red dextran (10 mg/mL; Invitrogen) to provide a fluorescent angiogram *in vivo*. Neural and vascular signals were recorded using a customized TPM (Ultima IV, Bruker Corporation, 500–550 nm (green), and 570–620 nm (red)) coupled with a Femto Second laser (Chameleon Ultra II, Coherent Inc. model-locked Ti: Sapphire laser) which generated two-photon excitation at 920 nm, equipped with a 16x (numerical aperture = 0.8) water-immersion objective (Olympus). PMT settings were kept constant for each experiment, but laser power was adjusted as required and was regulated by Pockels Cells (Conoptics). For functional imaging, the frame size was 375.47μm × 375.47 μm (pixels: 512 × 512) and the image was obtained at 30Hz in the resonant-galvo scanner (resonance frequency 8 KHz). For Structural imaging, the neurons and vascular in galvo-galvo system were imaged at 1024 × 1024 pixels of 375.47μm × 375.47 μm with 1Hz scanning velocity.

2.10. MRI

In MRI experiment, one cat (weight 3.1 kg) with hydrogel-elastomer neural interface and contralateral metal electrode was given sufentanil (2–4 μg/kg per hour i. v.) and 1.5%–2% isoflurane to maintain anesthesia. The intubation tube was connected to a ventilator and life support system. The cat was fixed on the scanning frame, and plasticine used to raise the animal's head so that the coil was firmly above the head. Stabilization of the imaging of the target area was achieved to avoid any movement during the scanning process.

MRI data were acquired on a 7-T research scanner (Siemens Healthcare, Erlangen, Germany) equipped with a whole-body gradient set (70 mT/m and 200 T/m per second), with a QED coil (Mayfield VillageOH, USA) for transmission and signal reception.

Structural images were obtained at a voxel size of 0.3-mm isotropic cube with 2D fast spin echo sequence (Turbo Spin Echo, TSE) [echo time (TE), 12 ms; repetition time (TR), 2000 ms; FOV, 510 × 420; averages, 32; bandwidth 284 Hz/Px; Echo spacing 11.5 ms; 20 slices].

2.10.1. Electrode's impedance measurement

Immerse the hydrogel electrode into a saline electrolyte containing the reference electrode of instrument. Silver wine was interconnected with a probe tip impedance measurement. Same measurement as PDMS dielectric shell (OmegaZ, World Precision Instruments, Inc. USA).

2.10.2. Data processing

All electrophysiological signaling data were analyzed using MATLAB (R2020b; MathWorks, US) toolbox of Chronux (http://chronux.org). For spectrum analysis, we applied the previous method of ECoG signal analysis ([45]). For surface vessels, imaging data were reconstructed and analyzed using ImageJ and MATLAB. MATLAB scripts were used to track the vascular skeleton and to quantify the length, intensity and branches of the vessels. Due to the limitation of imaging conditions, we selected an electrode center site (0.4*0.4 mm) and four sides surrounding areas (0.4*0.4 mm) to observe the changes caused by long-term electrode implantation. We demonstrated the overall blood vessel alternations by using the ratios of blood vessel characteristics of each part (surrounding the electrode) to those from the electrode site.

For calcium imaging motion correction, images were processed using Image Stabilizer (http://www.cs.cmu.edu/~kangli/code/Image_Stabilizer.html). ROIs were drawn around each visible neuron on a maximum intensity projection of the time course. For each FOV, 1-2 additional ROIs were drawn in areas without neurons to correct for background fluorescent intensity (F_0). Ca^{2+} signals were calculated as $\triangle F/F = (F - F_0)/F_0$, where F_0 represents baseline fluorescence and F represents the fluorescence at time t.

2.10.3. Statistical analysis

All data sets were first determined whether they are normal distribution by Shapiro-Wilk test. When data fitted normal distribution, One-way ANOVA followed by Tukey post hoc test was used to determine statistical differences. When data were not normal distribution, Kruskal-Wallis followed by Dunn's post hoc test or Mann-Whitney test was used.

Data were analyzed with GraphPad Prism 6 or SPSS software. Statistical significance was * $p < 0.05$, ** $p < 0.01$, *** $p < 0.001$ **** $p < 0.0001$.

3. Results

3.1. The fabrication and electrical characterization of hydrogel-elastomer neural interface

A 1 cm × 2 cm subdural neural interface was fabricated by using a hydrogel as an ionic conductor (impedance: 0.02 MΩ) and an elastomer as a dielectric (impedance: infinite) and the whole interface was at 500 μm thick which included the PDMS cover at 150 μm thick, the PDMS substrate at 300 μm thick and a thin layer of PDMS for adhering the cover to the substrate (Fig. 1B). After casting a polydimethylsiloxane (PDMS) substrate with three channels for three pairs of interconnected electrodes, we placed a silver ring at the end of each channel, and covered the channels with a layer of PDMS (Fig. 2A and B). The width of the channel was 1 mm and the depth was 150 μm. The pillar for placing the silver interconnect was 1.5 mm in diameter and the silver interconnect which was at 100 μm thick. The whole PDMS substrate was submerged in a solution of polyvinyl alcohol (PVA) and ACSF, drew the solution into the channels using a vacuum pump, and gelled the solution by freezing and thawing. The recording hydrogel electrodes with 1 mm diameter were linked through the hydrogel interconnectors to the silver rings on the edge of the interface. The PDMS top layer exposes the hydrogel electrodes but covers the hydrogel interconnectors and silver rings. Silver ring is only placed at the edge of the neural interface and does not directly contact the brain tissue. Consequently, our neural interface is much softer than metal electrodes.

We characterized the hydrogel-elastomer neural interface by submerging it in saline, applying an electrical stimulation to a hydrogel electrode, and recording the signal from the silver ring (Fig. 2C and D). The recorded voltage did not decay when the frequency of stimulation was below 100 Hz.

(A) Photo of PDMS substrate. (B) Steps of fabrication. 1. Use of a metal mold to cast a PDMS substrate with three channels. 2. Placement of a silver ring at the end of each channel. 3. Adherence of a PDMS cover to the substrate using a PDMS precursor. 4. Submergence of the PDMS structure into a precursor of PVA hydrogels with use of a vacuum pump to suck the precursor into the channels, and gelling of the PVA by freezing and thawing. (C) Experimental setup. (D) The detected voltages at different frequencies. Signals remain undistorted when the frequency is below 100 Hz.

3.2. The quality of long-term electrophysiological recording via hydrogel-elastomer neural interface

Next, we implanted the hydrogel-elastomer neural interface on one hemisphere of the cerebral cortex of a cat, and two commercial metal (platinum-iridium alloy) electrodes as control on the other hemisphere (Fig. 3A and B). A stimulating electrode made of tungsten was then inserted in the parietal lobe of the cortex on the hemisphere with the metal electrodes. We use a total of five electrodes to record the local field potential simultaneously. The cat was placed under isoflurane (ISO) (0.5%–0.8%), ISO (2%–3%), propofol (3–5 mg/kg/h), and propofol (10 mg/kg/h). The spectrums recorded by the hydrogel electrodes were comparable to those recorded by the metal electrodes under different

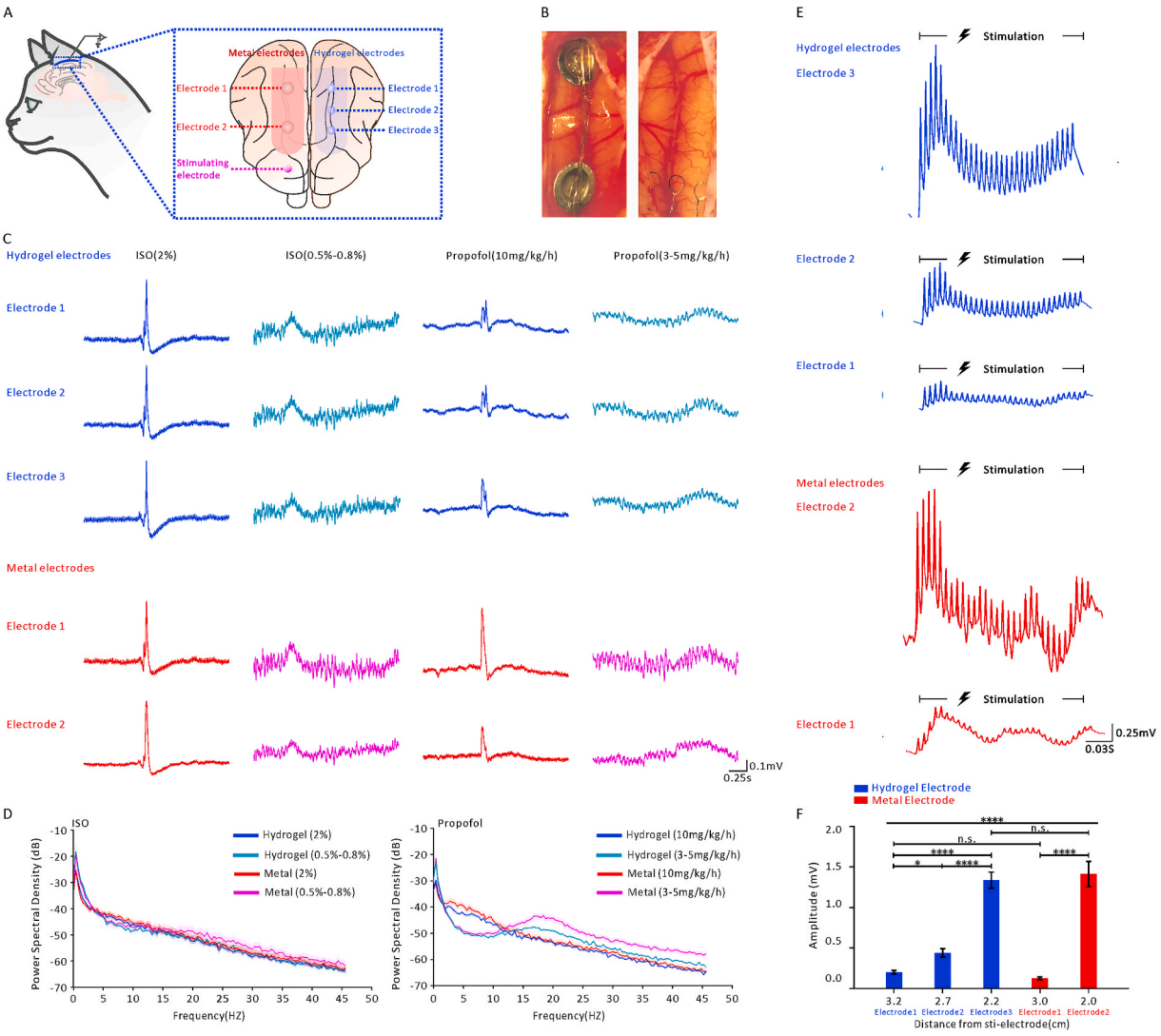

Fig. 3. Hydrogel electrodes and metal electrodes implanted in a cat.

dosages of ISO and propofol anesthesia in all bands excepting a significant difference of power spectral density was observed between hydrogel and metal electrodes at gamma band under propofol anesthesia (3–5 mg/kg/h) (Fig. 3D and fig. S1) ([4]). This phenomenon might be caused by propofol affects LFP energy at different brain areas distinctly and the disparity of exact recording locations between hydrogel and metal electrodes ([46]). Notably, comparable to metal electrodes, ECoG recorded by hydrogel electrodes showed significant differences between different anesthetic dosages at delta band. Similarly, significant differences of ECoG spectral power between different dosages of propofol anesthesia were observed at theta and beta bands. These results suggested that the quality of electrophysiological recordings from hydrogel electrodes is indeed similar to traditional metal electrodes.

We then used the five electrodes to record the responses to stimulation from the tungsten electrode (Fig. 3E). The hydrogel and metal electrodes recorded traces of a consistent pattern, but the amplitudes of the five traces differed depending on distances of the individual recording electrodes from the stimulating electrode. The further the recording electrode was from the stimulating electrode, the smaller the amplitude measured by the recording electrode (Fig. 3F). These results indicate that the hydrogel and metal electrodes have a comparable capability for electrophysiological recording. The quality of the signals recorded on the first day of implantation to those four weeks after was further compared (Fig. S2). Both recordings by the hydrogel and metal electrodes show negligible change over time.

(A) Three hydrogel electrodes and two metal electrodes were attached to the two hemispheres of the brain of a cat. Also attached is an electrode for stimulation. (B) A photo of the five implanted electrodes. (C) When the cat was under ISO or propofol anesthesia, the hydrogel electrodes and metal electrodes were used to record the local field potentials. (D) The power spectral density of ECoG signals under different dosages of ISO or propofol anesthesia. Data were collected from two cats. (E) Local field potential recorded by the hydrogel electrodes and metal electrodes when the cat was under 4 mg/kg/h propofol anesthesia and was stimulated with a current of amplitude 0.1 mA and frequency 200 Hz. (F) The peak-valley amplitudes of voltage recorded by the five electrodes (n = 30 pulses, data were collected from one cat *P < 0.05, ****P < 0.0001, Kruskal-Wallis test with Dunn's post hoc test.). Also listed are the distances in cm from the stimulating electrode to the five recording electrodes.

3.3. *The hydrogel-elastomer neural interface incurs much less glial reaction and cerebrovascular destruction than the metal electrode does*

We then compared the biocompatibility of the hydrogel and metal electrodes using angiography and immunohistochemistry (Fig. 4). Using the near infrared II (NIR-II) fluorescence microscopy ([44,47–49]), the

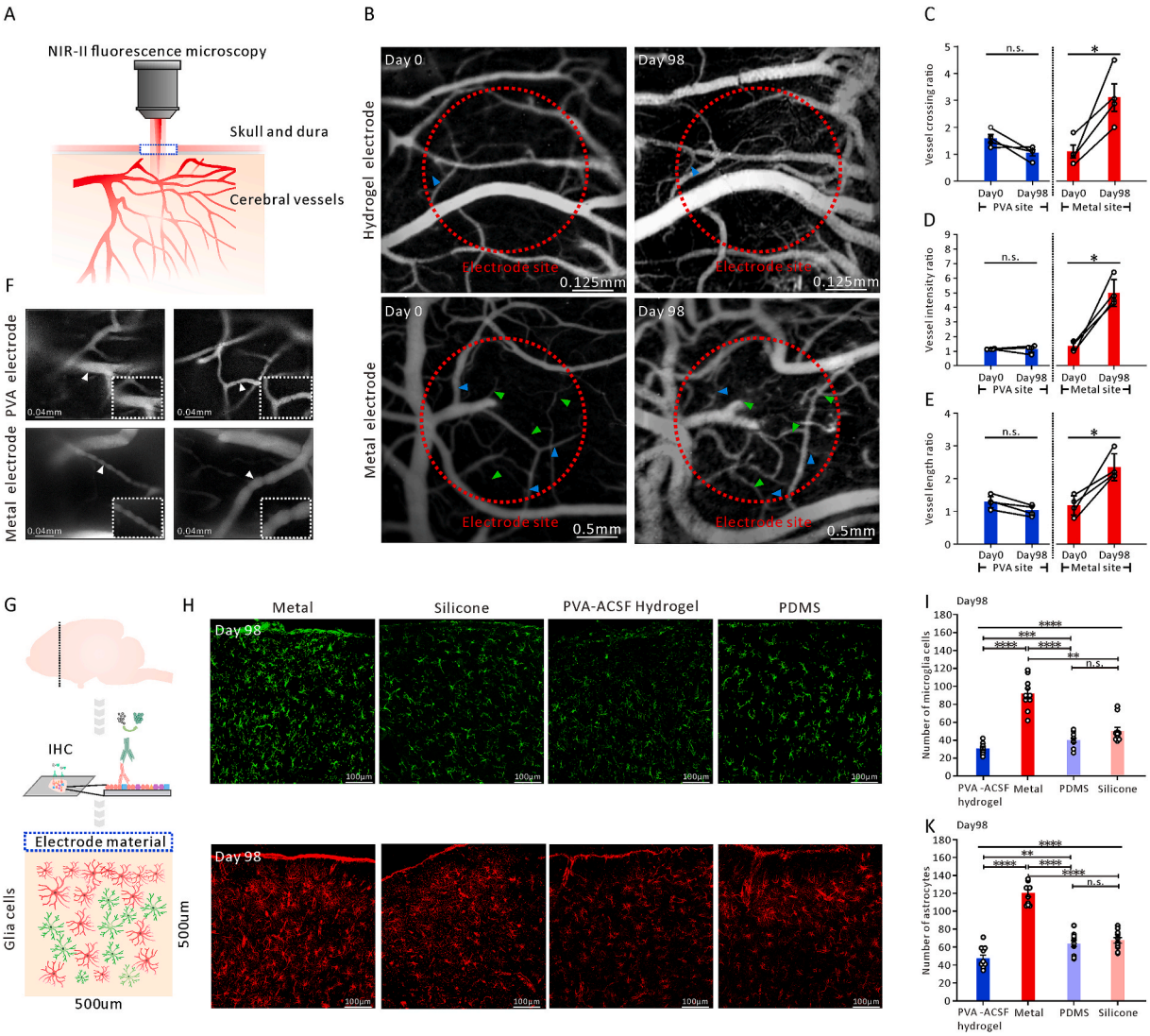

Fig. 4. Biocompatibility of the hydrogel and metal electrodes.

effects of the electrodes on cerebral vessels were investigated (Fig. 4A). After 98 days of implantation, the metal electrodes caused far more cerebrovascular changes than the hydrogel electrodes (Fig. 4B). We quantified the cerebrovascular changes using the crossing ratio, intensity ratio, and length ratio (Fig. 4C–E and see Materials and Methods). The fine cerebrovascular changes of the deep brain were also imaged (Fig. 4F). Distortion of vessels and expansion of vascular walls are observed beneath the metal electrodes, but not beneath the hydrogel electrodes. These findings indicate that the metal electrodes greatly alter the cerebral vessels both on the cortical surface and deep in the brain. Hydrogel electrodes, however, negligibly altered the cerebral vessels. We further compared the immune responses to the hydrogel and metal electrodes after 2, 3, 4 and 14 weeks of implantation. The numbers of activated glial cells (microglia and astrocytes) beneath the hydrogel electrodes are significantly fewer than those beneath the metal electrodes (Fig. 4G–K and fig. S3).

(A) Schematic of angiography using near infrared II fluorescence microscopy. (B) Angiographs taken on the surface of the brain before and after the implantation of the hydrogel and metal electrodes. (C-E) Geometric changes of cerebral vessels beneath the hydrogel and metal electrodes (n = 4 cerebral cortical areas surrounding the electrodes from one cat, Mann-Whitney test was used and *P < 0.5). (F) Angiographs taken at 0.4 mm beneath the electrodes. (G-K) Immunohistochemistry of microglia cells and astrocytes. For Fig. 4I, Kruskal-Wallis test with Dunn's post hoc test were used (**P < 0.05, ***P < 0.001 ****P < 0.0001, n = 10 or 11 brain slices from one cat). For Fig. 4K, One-way ANOVA test with Tukey's post hoc test were used (**P < 0.05, ****P < 0.0001, n = 10 or 11 brain slices from one cat).

3.4. *The hydrogel-elastomer neural interface enables simultaneous electrical recording and optical imaging*

Whereas metal electrodes are opaque, the hydrogel electrodes are highly transparent. This high transparency enables the hydrogel-elastomer neural interface to be used simultaneously for both electrical recording and optical imaging. We fabricated a 5 mm × 7 mm neural interface of two hydrogel electrodes and attached this interface to the cortical surface of a mouse (Fig. 5A). Then we used two-photon microscopy to observe calcium signals of neurons and cerebral vessels beneath an individual hydrogel electrode (Fig. 5B). Such a soft and transparent neural interface opens the door to study long-term neurovascular coupling between the neural circuit and the vascular system.

As the mouse was stimulated with a single pulse or multi-pulse *via* an electrode attached at the front left paw, we recorded the calcium signal in layer II of somatosensory cortex using two-photon microscopy (Fig. 5C). The simultaneous electrical recording and optical imagining showed the relationships between electrical signals and calcium (Fig. 5D and E). While the local field potential averages the electrical signals of

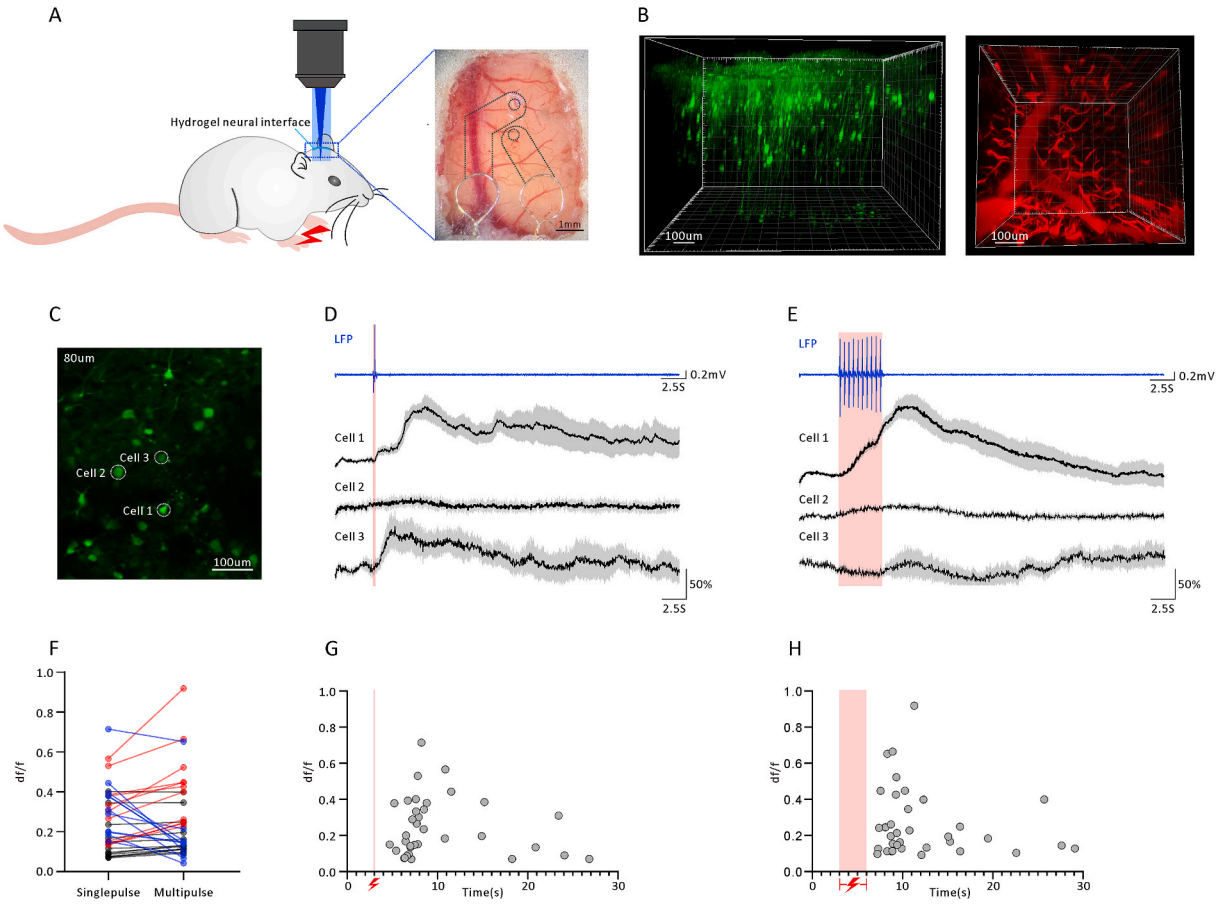

Fig. 5. The hydrogel-elastomer neural interface enables simultaneous electrical recording and optical imaging. (A) An interface of two hydrogel electrodes was attached to the cortical surface of a mouse. In the photo, the hydrogel electrodes and interconnects are transparent and are outlined using dashed lines. (B) Three-dimensional reconstruction of cortical neurons and cerebral vessels. (C) Calcium image of neurons at depth of 80 μm before electrical stimulation at the left front paw. (D–E) The local field potential and the brightness of three neurons as a function of time after a single pulse and multi-pulses of electrical stimulation. (F) The brightness change of 35 pair neurons after single/multi-pulse electrical stimulation (red representing an increase of more than 5%, blue representing a decrease of more than 5%, grey representing a change within 5%). (G–H) Scatter plot of 35 cells from 6 mice between time to peak brightness of calcium fluorescence and the peaks after two patterns of electrical stimulation. (For interpretation of the references to colour in this figure legend, the reader is referred to the Web version of this article.)

many cells, the calcium signals could be optically observed for individual cells. Either single pulse electro stimulation or multi-pulse (a train of pulses) electro stimulation modes was applied. The local field potential delayed little from the stimulation signal, but the calcium signal exhibited various responses. For example, the calcium signal peak increase in multi-pulse stimulation for Cell 1, kept steady for Cell 2, and decreased somewhat for Cell 3 after comparison of single-pulse stimulation. The probability of the three changes in 35 neurons was equivalent, which also shows that different stimulation modes have little effect on neurons (Fig. 5F). These two types of stimulations cause similar

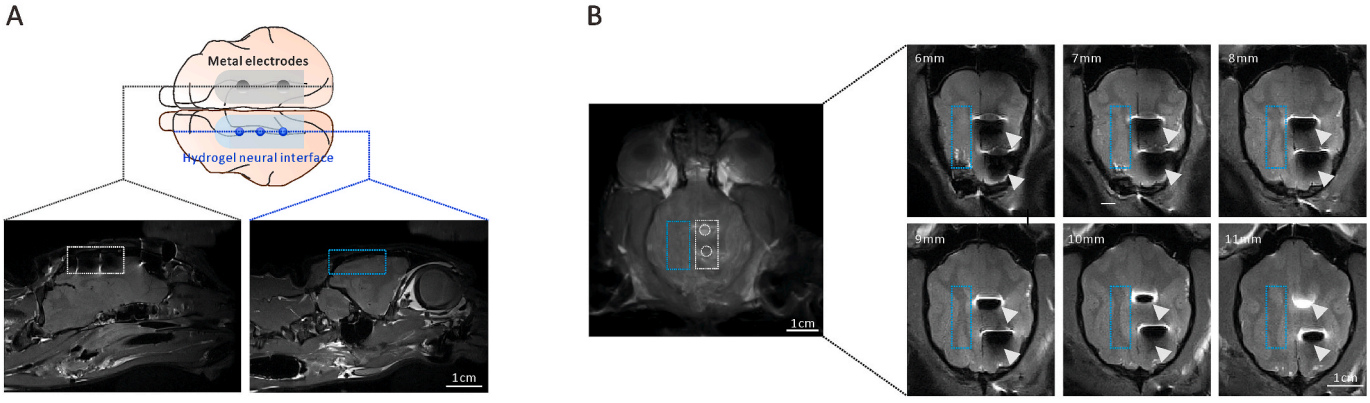

Fig. 6. Hydrogel neural interface is compatible with magnetic resonance imagining. (A) The MRI of a cat with two metal electrodes and three hydrogel electrodes attached on the two hemispheres of the brain. (B) The MRI scans at the various indicated depths of the brain.

distributions of calcium signals (Fig. 5G and H).

3.5. Hydrogel neural interface is compatible with magnetic resonance imagining

We also demonstrated that the hydrogel neural interface was compatible with magnetic resonance imaging by performing 7T MRI scanning on the cat implanted with two metal electrodes and three hydrogel electrodes. The sagittal plane scan shows that the metal electrodes cause image artifacts (in the white frame), but the hydrogel electrodes did not cause image artifacts (in the blue frame) (Fig. 6A). The transverse plane scan shows similar observations (Fig. 6B). Furthermore, the metal electrodes caused image artifacts in the transverse planes deep in the brain.

4. Conclusions

In summary, we have developed a soft, multimodal, subdural neural interface by integrating a hydrogel and an elastomer. The interface is mechanically compatible with the brain, the hydrogel being comparable to the brain tissue, and the elastomer is comparable to dura mater. The biocompatibility, demonstrated by immunohistochemistry and angiography, enables the hydrogel-elastomer neural interface to function *in vivo* for a long period. The optical transparency of the interface enables simultaneous electrical recording and optical imaging. We have demonstrated the simultaneous collection of local field potentials, cerebrovascular images, and single-cell calcium signals. Unlike metal electrodes, the hydrogel interface does not produce artifact images in MRI. The hydrogel-elastomer neural interface is compatible with other advanced techniques in neurobiology, such as optogenetic stimulation and functional MRI. The interface provides a new tool to integrate information of various types, across scales. An immediate opportunity is to study the neurovascular coupling between the neural circuit and vascular system over a long period. The interface also opens doors to clinical applications. For example, an epileptic patient implanted with the soft electrode can be examined by MRI. The long-term soft electrodes can also be used to decode brain signals for artificial limbs.

Credit author statement

Xiaomeng Wang: Conceptualization, Methodology, Investigation, Writing – original draft preparation. **Mengqi Wang**: Investigation, Writing – original draft preparation. **Hao Sheng**: Conceptualization, Methodology. **Liang Zhu**: Data curation. **Junming Zhu**: Methodology. **Hequn Zhang**: Data curation. **Yin Liu**: Data curation. **Li Zhan**: Data Formal analysis. **Xi Wang**: Data curation. **Jiaozhen Zhang**: Data curation. **Xiaotong Wu**: Data Formal analysis. **Zhigang Suo**: Conceptualization, Supervision, Writing – original draft preparation, Funding acquisition. **Wang Xi**: Methodology, Software, Supervision, Writing-Reviewing and Editing, Funding acquisition. **Hao Wang**: Conceptualization, Supervision, Writing- Reviewing and Editing, Funding acquisition.

Funding

This work was supported by grants from the National Natural Science Foundation of China (31970940, 31622027, 31671100, 91632105 and 81961128029), the Zhejiang Provincial Natural Science Foundation of China (LR18H090001), the Non-profit Central Research Institute Fund of the Chinese Academy of Medical Sciences (2018PT31041), the Program for Introducing Talents in Discipline to Universities, and the Fundamental Research Funds for Central Universities (2021FZZX001-37). Zhejiang Lab (No. 2018EB0ZX01). ZS acknowledges the support of the NSF MRSEC at Harvard (DMR-14-20,570).

Author contributions

H·W., W.X., H·S and X.M.W. designed experiments; M.Q.W., X.M.W., L.Z. and H.S. performed the experiments; and Z.G.S., H·W., W.X., H·S and X.M.W. and M.Q.W. wrote the paper.

Data and materials availability

All data is available in the main text or the supplementary materials.

Declaration of competing interest

The authors declare the following financial interests/personal relationships which may be considered as potential competing interests: Hao Wang has patent #ZL 2017 1 0806112.X issued to Zhejiang University. Hao Sheng has patent #ZL 2017 1 0806112.X issued to Zhejiang University.

Acknowledgments

We thank Dr. Jun Qian of the Zhejiang University Optical department for his kind help with the NIR-II imaging tools and Dr. Ruiliang Ba and Dr. Xiaotong Zhang of ZIINT for their kind help with the MRI imaging experiment. We thank Chris Wood of the Zhejiang University Life Science College for critical comments on this manuscript.

Appendix A. Supplementary data

Supplementary data to this article can be found online at https://doi.org/10.1016/j.biomaterials.2021.121352.

References

[1] G. Buzsáki, C.A. Anastassiou, C. Koch, The origin of extracellular fields and currents-EEG, ECoG, LFP and spikes, Nat. Rev. Neurosci. 13 (2012) 407–420.
[2] S.P. Lacour, G. Courtine, J. Guck, Materials and technologies for soft implantable neuroprostheses, Nat. Rev. Mater. 1 (2016) 16063.
[3] P. Moshayedi, et al., The relationship between glial cell mechanosensitivity and foreign body reactions in the central nervous system, Biomaterials 35 (2014) 3919–3925.
[4] G. Buzsáki, A. Draguhn, Neuronal oscillations in cortical networks, Science (New York, N.Y.) 304 (2004) 1926–1929.
[5] S. Kellis, B. Greger, S. Hanrahan, P. House, R. Brown, Sensing Millimeter-Scale Dynamics in Cortical Surface Potentials for Neural Prosthetics, IEEE, 2011.
[6] E.C. Leuthardt, Z. Freudenberg, D. Bundy, J. Roland, Microscale recording from human motor cortex: implications for minimally invasive electrocorticographic brain-computer interfaces, Neurosurg. Focus 27 (2009) E10.
[7] J.D. Breshears, et al., Decoding motor signals from the pediatric cortex: implications for brain-computer interfaces in children, Pediatrics 128 (2011) e160–168.
[8] E.C. Leuthardt, G. Schalk, J.R. Wolpaw, J.G. Ojemann, D.W. Moran, A brain-computer interface using electrocorticographic signals in humans, J. Neural. Eng. 1 (2004) 63–71.
[9] C.H. Chiang, et al., Flexible, high-resolution thin-film electrodes for human and animal neural research, J. Neural. Eng. 18 (2021).
[10] S. Kellis, B. Greger, S. Hanrahan, P. House, R. Brown, Platinum microwire for subdural electrocorticography over human neocortex: millimeter-scale spatiotemporal dynamics, Ann. Int. Conf. IEEE Eng. Med. Biol. Soc. (2011) 4761–4765. IEEE Engineering in Medicine and Biology Society. Annual International Conference 2011.
[11] J. Parvizi, S. Kastner, Promises and limitations of human intracranial electroencephalography, Nat. Neurosci. 21 (2018) 474–483.
[12] R.W. Griffith, D.R. Humphrey, Long-term gliosis around chronically implanted platinum electrodes in the Rhesus macaque motor cortex, Neurosci. Lett. 406 (2006) 81–86.
[13] R. Feiner, T.J.N.R.M. Dvir, Tissue–electronics Interfaces: from Implantable Devices to Engineered Tissues, vol. 3, 2017, p. 17076.
[14] J. Liu, et al., Syringe-injectable electronics, Nat. Nanotechnol. 10 (2015) 629–636.
[15] Y. Chen, et al., How is flexible electronics advancing neuroscience research? Biomaterials 268 (2021), 120559.
[16] L. Luan, et al., Recent advances in electrical neural interface engineering: minimal invasiveness, longevity, and scalability, Neuron 108 (2020) 302–321.
[17] K. Xiao, C. Wan, L. Jiang, X. Chen, M. Antonietti, Bioinspired ionic sensory systems: the successor of electronics, Adv. Mat. (Deerfield Beach, Fla.) 32 (2020), e2000218.

[18] D. Khodagholy, et al., Highly conformable conducting polymer electrodes for in vivo recordings, Adv. Mat. (Deerfield Beach, Fla.) 23 (2011) H268–H272.
[19] D. Khodagholy, et al., NeuroGrid: recording action potentials from the surface of the brain, Nat. Neurosci. 18 (2015) 310–315.
[20] Ivan, et al., Biomaterials. Electronic Dura Mater for Long-Term Multimodal Neural Interfaces, 2015.
[21] G. Schiavone, et al., Guidelines to study and develop soft electrode systems for neural stimulation, Neuron 108 (2020) 238–258.
[22] C.M. Tringides, et al., Viscoelastic surface electrode arrays to interface with viscoelastic tissues, Nat. Nanotechnol. (2021).
[23] H. Yuk, B. Lu, X.J.C.S.R. Zhao, Hydrogel Bioelectr. 48 (2018).
[24] Y. Liu, et al., Soft and elastic hydrogel-based microelectronics for localized low-voltage neuromodulation, Nat. Biomed. Eng. 3 (2019) 58–68.
[25] Y. Lu, et al., Poly(3,4-ethylenedioxythiophene)/poly(styrenesulfonate)-poly(vinyl alcohol)/poly(acrylic acid) interpenetrating polymer networks for improving optrode-neural tissue interface in optogenetics, Biomaterials 33 (2012) 378–394.
[26] A.M. Oros-Peusquens, R. Louçã o, M. Zimmermann, K.J. Langen, N.J. Shah, Methods for molecular imaging of brain tumours in a hybrid MR-PET context: water content, T(2)(*), diffusion indices and FET-PET, Methods (San Diego, Calif.) 130 (2017) 135–151.
[27] K.P. Whittall, et al., In vivo measurement of T2 distributions and water contents in normal human brain, Magn. Reson. Med. 37 (1997) 34–43.
[28] S.J. Nagel, et al., Spinal dura mater: biophysical characteristics relevant to medical device development, J. Med. Eng. Technol. 42 (2018) 128–139.
[29] H. Ozawa, T. Matsumoto, T. Ohashi, M. Sato, S. Kokubun, Mechanical properties and function of the spinal pia mater, J. Neurosurg. Spine 1 (2004) 122–127.
[30] K.Y. Kwon, B. Sirowatka, A. Weber, W. Li, Opto- μECoG array: a hybrid neural interface with transparent μECoG electrode array and integrated LEDs for optogenetics, IEEE Transac. Biomed. Circuit Syst. 7 (2013) 593–600.
[31] N. Kunori, I. Takashima, A transparent epidural electrode array for use in conjunction with optical imaging, J. Neurosci. Methods 251 (2015) 130–137.
[32] L. Wang, et al., Ultrasoft and Highly Stretchable Hydrogel Optical Fibers for in Vivo Optogenetic Modulations, vol. **6**, 2018, p. 1800427.
[33] J. Viventi, et al., Flexible, foldable, actively multiplexed, high-density electrode array for mapping brain activity in vivo, Nat. Neurosci. 14 (2011) 1599–1605.
[34] J. Zhang, et al., Stretchable transparent electrode arrays for simultaneous electrical and optical interrogation of neural circuits in vivo, Nano Lett. 18 (2018) 2903–2911.
[35] T.I. Kim, et al., Injectable, cellular-scale optoelectronics with applications for wireless optogenetics, Science 340 (2013) 211–216.
[36] K. Tybrandt, et al., High-density stretchable electrode grids for chronic neural recording, Adv. Mat. (Deerfield Beach, Fla.) 30 (2018), e1706520.
[37] X. Gong, et al., An ultra-sensitive step-function opsin for minimally invasive optogenetic stimulation in mice and macaques, Neuron 107 (2020) 38–51.
[38] M. Thunemann, et al., Deep 2-photon imaging and artifact-free optogenetics through transparent graphene microelectrode arrays, Nat. Commun. 9 (2018) 2035.
[39] S. Zhao, et al., Graphene encapsulated copper microwires as highly MRI compatible neural electrodes, Nano Lett. 16 (2016) 7731–7738.
[40] L.M. Angelone, J. Ahveninen, J.W. Belliveau, G. Bonmassar, Analysis of the role of lead resistivity in specific absorption rate for deep brain stimulator leads at 3T MRI, IEEE Trans. Med. Imag. 29 (2010) 1029–1038.
[41] C.J. Sparrey, G.T. Manley, T.M. Keaveny, Effects of white, grey, and pia mater properties on tissue level stresses and strains in the compressed spinal cord, J. Neurotrauma 26 (2009) 585–595.
[42] S.P. Lacour, G. Courtine, J. Guck, Materials and technologies for soft implantable neuroprostheses, Nat. Rev. Mater. 1 (2016).
[43] A. Devor, et al., Suppressed neuronal activity and concurrent arteriolar vasoconstriction may explain negative blood oxygenation level-dependent signal, J. Neurosci. : Off. J. Soc. Neurosci. 27 (2007) 4452–4459.
[44] Z. Cai, et al., NIR-II fluorescence microscopic imaging of cortical vasculature in non-human primates, Theranostics 10 (2020) 4265–4276.
[45] J.D. Lendner, et al., An electrophysiological marker of arousal level in humans, Elife 9 (2020).
[46] Y. Ishizawa, et al., Dynamics of propofol-induced loss of consciousness across primate neocortex, J. Neurosci. : Off. J. Soc. Neurosci. 36 (2016) 7718–7726.
[47] G. Hong, A.L. Antaris, H. Dai, Near-infrared fluorophores for biomedical imaging, Nat. Biomed. Eng. 1 (2017).
[48] Z. Hu, et al., First-in-human liver-tumour surgery guided by multispectral fluorescence imaging in the visible and near-infrared-I/II windows, Nat. Biomed. Eng. 4 (2020) 259–271.
[49] Y. Zhong, et al., In vivo molecular imaging for immunotherapy using ultra-bright near-infrared-IIb rare-earth nanoparticles, Nat. Biotechnol. 37 (2019) 1322–1331.